PROCEEDINGS OF SCIENCE

1-Jettiness in DIS: Measuring 2 Jets in 3 Ways *

Daekyoung Kang†
Center for Theoretical Physics, Massachusetts Institute of Technology, Cambridge, MA 02139, USA
E-mail: kang1@mit.edu

Christopher Lee
Theoretical Division, MS B283, Los Alamos National Laboratory, Los Alamos, NM 87545, USA
E-mail: clee@lanl.gov

Iain W. Stewart
Center for Theoretical Physics, Massachusetts Institute of Technology, Cambridge, MA 02139, USA
E-mail: iains@mit.edu

We compute cross sections for two-jet production in deep inelastic scattering (DIS), with one jet from initial state radiation (ISR) and the other from final state radiation, with a summation of large logarithms up to next-to-next-to-leading logarithmic (NNLL) accuracy. Use of the DIS event shape 1-jettiness ensures that events have two well-collimated jets. We calculate distributions for three versions of 1-jettiness that have different sensitivity to the transverse momentum of the ISR, and derive factorization theorems for each of them using the soft collinear effective theory (SCET). The structure of the transverse momentum dependence in the factorization theorems is different for each 1-jettiness. We present numerical results for these three observables with parameters for the HERA collider.

XXI International Workshop on Deep-Inelastic Scattering and Related Subject -DIS2013,
22-26 April 2013
Marseilles,France

*LA-UR-13-26573, MIT-CTP 4488
†Speaker.

PoS(DIS 2013)158

Studying jet production with event shapes can be advantageous, since it is possible to achieve higher precision compared to exclusive jet cross sections defined with jet algorithms. In e^+e^- collisions a classical example is thrust $T = 1 - \tau$ [1], where the hadronic final state is constrained to two jets for small τ. Here results are available up to N^{3}LL+$\mathcal{O}(\alpha_s^3)$ [2, 3, 4, 5, 6, 7, 8, 9] and this allows $\sim 1\%$ level theoretical accuracy in α_s extractions. A version of DIS thrust has been studied in HERA experiments [10, 11, 12, 13, 14, 15] and was calculated in [16, 17] at NLL+$\mathcal{O}(\alpha_s^2)$ accuracy. However, the HERA definition of the DIS thrust introduces a technical obstacle in theoretical calculations beyond NLL accuracy because it leads to non-global logarithms and it is unknown how to resum these beyond the leading logs [17, 18]. To determine higher order results for the log resummation and to rigorously include power corrections it is useful to derive factorization theorems that account for results to all orders in perturbation theory as well as the leading power corrections. To do this we use the event shape 1-jettiness, which is a thrust-like event shape without non-global logarithms. We define three versions of 1-jettiness in Sec. 1, review results for the factorization theorems for these observables in Sec. 2, and give numerical results for 1-jettiness distributions up to NNLL accuracy in Sec. 3 [19].

1. 1-Jettiness for DIS

The 1-jettiness is a special case of N-jettiness introduced in Ref. [20]. The N-jettiness is a generalization of thrust and a small value of N-jettiness constrains the final state to contain $N+N_B$ jets where N_B is the number of initial state jets by ISR from proton beams and N is the number of final state jets. In DIS N_B is 1. In this paper we will focus on the case of a single final jet ($N = 1$), for which the DIS 1-jettiness observable is defined by

$$\tau_1 = \frac{2}{Q^2} \sum_{i \in X} \min\{q_B \cdot p_i, q_J \cdot p_i\}\,. \tag{1.1}$$

Here a four vector q_B points along the incident proton momentum and a four vector q_J is picked to determine an axis for the measurement of the final-state jet. The min chooses the smaller scalar product, and also groups all particles in the final state X into two regions, particles closer to q_B (smaller $q_B \cdot p_i$) and those closer to q_J (smaller $q_J \cdot p_i$). This grouping depends on the choice of q_B and q_J. We consider three different cases:

$$\tau_1^a: \qquad q_B^a = xP\,, \qquad\qquad q_J^a = \text{jet axis} \tag{1.2a}$$

$$\tau_1^b: \qquad q_B^b = xP\,, \qquad\qquad q_J^b = q + xP \tag{1.2b}$$

$$\tau_1^c: \qquad q_B^c = P\,, \qquad\qquad q_J^c = k\,, \tag{1.2c}$$

where P, k, and q are the initial proton, incoming electron, and virtual boson momenta, respectively, and $x = Q^2/(2P\cdot q)$ is the Björken scaling variable where $q^2 = -Q^2$. The three variants $\tau_1^{a,b,c}$ in Eq. (1.2) are named for the corresponding properties of the vector q_J. In τ_1^a, q_J^a is *aligned* with a jet axis that is defined either by a jet algorithm, or by a minimization of the 1-jettiness in Eq. (1.1) as in [21]. In τ_1^b, the vectors q_J^b and q_B^b are back-to-back in the *Breit frame*. τ_1^b can be rewritten in a way that is equivalent to one of the measured DIS thrust distributions except for the normalization [16, 19] and it could be analyzed with existing thrust data from the HERA experiment. Similarly, for τ_1^c the vectors q_B^c and q_J^c are back-to-back in the *center-of-momentum frame*.

2. Factorization Theorems for Different Jet Axes

All orders factorization theorems for the three versions of 1-jettiness in Eq. (1.2) can be used to obtain higher order resutls, and here we briefly describe them and highlight their differences. A complete derivation and further details can be found in [19]. A factorization theorem for τ_1^a also has been obtained in [22, 23]. The cross section for the three cases can be obtained as special cases of the general result

$$\frac{d\sigma}{dx\,dQ^2\,d\tau_1} = \frac{d\sigma_0}{dx\,dQ^2}\int dt_J\,dt_B\,dk_S\,d^2\mathbf{p}_\perp\,\delta\Big(\tau_1-\frac{t_J}{s_J}-\frac{t_B}{s_B}-\frac{k_S}{Q_R}\Big) \\ \times\sum_\kappa H_\kappa(Q^2,\mu)\,J_q(t_J-(\mathbf{q}_\perp+\mathbf{p}_\perp)^2,\mu)\,\mathscr{B}_{\kappa/p}(t_B,x,\mathbf{p}_\perp^2,\mu)\,S_{\rm hemi}(k_S,\mu)\,, \tag{2.1}$$

where σ_0 is the Born cross section, s_J, s_B, Q_R are normalization constants which are different for $\tau_1^{a,b,c}$ (see [19]), and κ is quark/antiquark flavors. H_κ is a hard function containing virtual corrections, and determined by matching QCD onto SCET. J_q is a quark jet function describing radiation of collinear quarks and gluons from an initial quark. $\mathscr{B}_{\kappa/p}$ is a quark beam function [24, 25, 26] with a perturbative kernel for collinear radiation and the parton distribution function (PDF) as

$$\mathscr{B}_{\kappa/p}(t_B,x,\mathbf{p}_\perp^2,\mu) = \sum_j\int_x^1\frac{dz}{z}\,\mathscr{I}_{\kappa j}\Big(t_B,\frac{x}{z},\mathbf{p}_\perp^2,\mu\Big)\,f_{j/p}(z,\mu), \tag{2.2}$$

where t_B is the transverse virtuality (p^+p^-) of the quark κ, and $\mathbf{p}_\perp$ is a transverse momentum of initial state radiation (ISR). $S_{\rm hemi}$ is the hemisphere soft function that describes radiation of soft particles from initial and final states. Note that $S_{\rm hemi}$ for the three observables $\tau_1^{a,b,c}$ is the same, which can be proved by using rescaling invariance of soft Wilson lines. Finally, $\mathbf{q}_\perp$ is the transverse momentum of the virtual boson respect to the jet and beam axes q_B and q_J in Eq. (1.1).

Eq. (2.1) has different transverse momentum dependencies for the three 1-jettinesses. In the case of τ_1^a, q_J is aligned with the jet axis and the argument of the jet function $t_J-(\mathbf{q}_\perp+\mathbf{p}_\perp)^2\to t_J$. Here the transverse integral acts on the beam function and it becomes the ordinary beam function defined in Ref. [24]. For τ_1^b, $\mathbf{q}_\perp$ is zero because q is written as a linear combination of $q_{B,J}$, but both J_q and $\mathscr{B}_{\kappa/p}$ involve $\mathbf{p}_\perp$. For τ_1^c there is no simplification from Eq. (2.1). Because of the different transverse momentum dependence in the beam function for τ_1^b and τ_1^c, the difference between these observables is sensitive to the transverse momentum of the ISR.

Hard, jet, beam, and soft functions in Eq. (2.1) each depend on a factorization scale μ (which is also precisely the renormalization scale in SCET). These functions contains logs of μ^2/Q^2, $\mu^2/(\tau_1 Q^2)$, or $\mu^2/(\tau_1^2 Q^2)$ and there are always large logs when $\tau_1 \ll 1$. The large logs should be resummed to achieve accurate prediction and this is achieved by using renormalization group evolution (RGE) in SCET. Each function is evolved from the natural scale $\mu_{H,J,B,S}$ where its logs are minimized to a common (arbitrary) scale μ. This sums up towers of logs of τ_1 to all order in α_s. The logarithmic accuracy of the resummation is determined by the α_s order of the anomalous dimensions. In this paper, our result of 1-jettiness is given to NNLL accuracy which requires 3-loop cusp anomalous dimension, 2-loop anomalous dimensions, and complete 1-loop results for the hard, jet, beam, and soft functions.

Nonperturbative effects in the soft function from gluons with momenta $\sim\Lambda_{\rm QCD}$ can be accounted for via a shape function. To illustrate how the nonperturbative effect deforms perturbative

PoS(DIS 2013)158

result, we adopt a simple model function for the peak region ($\tau_1 \sim 2\Lambda_{\rm QCD}/Q$). In the tail region ($2\Lambda_{\rm QCD}/Q \ll \tau_1 \ll 1$) the universality of the leading nonperturbative corrections has been shown for various e^+e^- event shapes and collision energies [27, 28, 29, 30] (for earlier work see [31, 32, 33]). This universality is also valid for power corrections for the three results considered in Eq. (2.1). In the tail region, the dominant power corrections are determined by a single parameter $\Omega_1^{a,b,c}$ as

$$\frac{d\sigma}{d\tau_1} = \frac{d\sigma^{\rm pert}}{d\tau_1} - \frac{2\Omega_1}{Q_R}\frac{d^2\sigma^{\rm pert}}{d\tau_1^2} + \cdots , \tag{2.3}$$

where we leave x and Q dependencies in the cross section implicit. Note that Ω_1 is rigorously defined as a matrix element of a product of soft Wilson lines. In Ref. [19], we proved the universality of Ω_1 for the three 1-jettinesses in the presence of hadron mass effects:

$$\Omega_1 = \Omega_1^{\rm a} = \Omega_1^{\rm b} = \Omega_1^{\rm c} . \tag{2.4}$$

This prediction can be tested experimentally.

3. Numerical results at NNLL

Lets consider numerical results for the three 1-jettiness: τ_1^a, τ_1^b, and τ_1^c. The results are accurate for small τ_1, and are resummed to LL, NLL, or NNLL accuracy, and also include the singular terms at fixed order $\mathcal{O}(\alpha_s)$. We present the τ_1^a spectra first, and then compare τ_1^b and τ_1^c spectra to τ_1^a. For the total invariant mass the value $s = (300\ \mathrm{GeV})^2$ in the H1 and ZEUS experiments is used. We also present cumulant cross sections $\sigma_c(\tau_1)$ which are defined as

$$\sigma_c(\tau_1, x, Q^2) = \frac{1}{\sigma_0}\int_0^{\tau_1} d\tau_1' \frac{d\sigma}{dx\,dQ^2\,d\tau_1'} , \tag{3.1}$$

where σ_0 is the Born cross section.

In the calculations of Eq. (3.1), the matrix elements H, J, B, and, S are evaluated at their natural scales $\mu_{H,B,J,S}$, at which logarithms in their fixed order calculations are minimized, and are then evolved to a common scale μ. For example, the natural scale for μ_S is $\tau_1 Q$. The evolution sums up $\log\tau_1$ terms, which is important when $\tau_1 \ll 1$. For very small $\tau_1 \sim \Lambda_{\rm QCD}/Q$ the scale μ_S approaches the nonperturbative region, and for values in this region must be frozen at a fixed scale $\sim 1\,\mathrm{GeV}$ since otherwise the perturbative expansion for the soft functions anomalous dimension fails. For large $\tau_1 \sim 1$ the logs are not large and the resummation must be turned off so that the fixed order NLO result is reproduced. The scales $\mu_{H,B,J,S}$ must change with τ_1 to meet these requirements, which is achieved with "profile functions" which are used for the results in Fig. 1 and Fig. 2. Perturbative uncertainties are computed by varying all scales up/down by factors of 2, as well as by other independent variations of the various scales, and the uncertainty from these variations decrease as the order in resummed perturbation theory increases. Explicit expressions of the profile functions and the variations used are given in Ref. [19].

Fig. 1 shows the τ_1^a cumulant (Left) and differential (Right) distribution at $Q = 80$ GeV and $x = 0.2$. Three curves represent the results resummed to LL, NLL, and NNLL accuracy and their perturbative uncertainty bands. The plot shows an excellent order-by-order convergence from LL

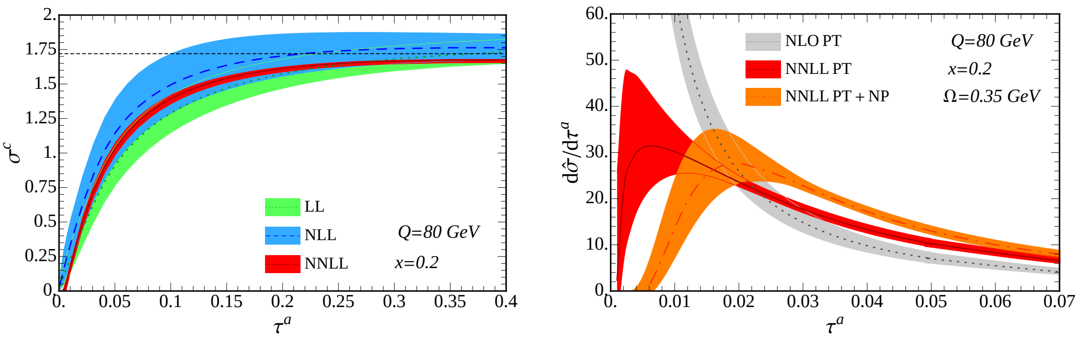

Figure 1: Left: Cumulant distribution in τ_1^a. Colored bands and central lines show theoretical uncertainties and central values to LL (dotted line, green band), NLL (dashed line, blue band), and NNLL (solid line, red band) accuracy and the horizontal dashed line is the total cross section. Right: Differential distribution in τ_1^a in the peak region, NNLL with nonperturbative shape function taken into account (NNLL PT+NP, dashed, orange), and without NP shape function at fixed-order α_s (NLO PT, dotted, gray) and resummed (NNLL PT, solid, red).

to NNLL order. One also finds only a small difference between the total cross section at $\mathcal{O}(\alpha_s)$ (dashed horizontal line) and the NNLL cumulant at large τ_1^a, indicating that the singular terms dominate. (The remaining difference estimates the size of the small nonsingular terms not taken into account in this work.) In the differential distribution, the NNLL result with and without nonperturbative effects (NNLL PT + NP and NNLL PT) is presented in comparison with purely fixed-order NLO results (NLO PT). For the purpose of illustrating the nonperturbative effect, we use the simplest shape function with a single basis function and $\Omega_1 = 0.35$ GeV for the nonperturbative parameter and convolved the perturbative cross section with the shape function. The dominant effect is a shift to the cross section's τ_1^a value. Above the peak region this correction reduces to the simple power correction in Eq. (2.3) determined by $\Omega_1 \sim \mathcal{O}(\Lambda_{\rm QCD}/\tau_1 Q)$. For a more realistic peak region analysis, a shape function with more basis functions should be used and parameters in the basis should be determined from experimental data. In the endpoint region, the NLO result blows up while the NNLL result is well behaved due to the resummation of large logs.

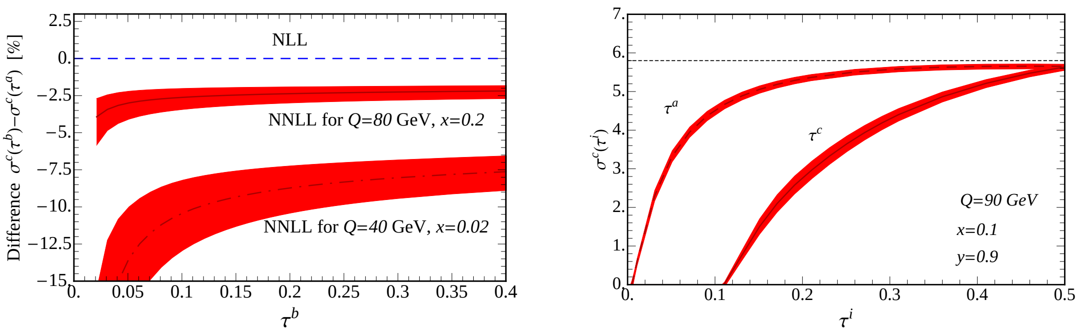

Figure 2: Left: Difference between τ_1^b and τ_1^a cumulant distributions at 2 sets of Q and x. The difference vanishes at NLL accuracy. Right: τ_1^c cumulant distribution in comparison to τ_1^a distribution. Notice that τ_1^c distribution has a threshold at $1-y=0.1$. The horizontal dashed line is the total cross section.

The τ_1^b cross section differs from τ_1^a by a single term at NLO, which contains $\ln z$. The term is convolved with PDF and integrated over from x to 1 and its contribution to the cross section is larger for smaller x. This is shown in the left panel in Fig. 2, which displays the percent difference at NNLL for two sets of (Q,x) values: $(80\text{ GeV}, 0.2)$ and $(40\text{ GeV}, 0.02)$. For $x = 0.2$ the size of the difference is a few percent, which is small compared to that for smaller $x = 0.02$. The difference goes up to 10-15% at $x = 0.02$. This difference is not sensitive to Q, because of the moderate Q dependence in the cross section. Note that τ_1^a and τ_1^b do not differ at NLL because both their NLL logs and LO cross sections are the same.

The 1-jettiness τ_1^c measures a jet close to the z axis (incoming electron direction) in the CM frame and the factorization theorem in Eq. (2.1) is valid for a jet with small transverse momentum $q_\perp^2 = (1-y)Q^2 \ll Q^2$. By the relation $y = Q^2/xs$ this means that values of Q and x should be chosen to satisfy $1-y \ll 1$. Here, we use $Q = 90$ GeV and $x = 0.1$ which corresponds to $y = 0.9$. The right panel in Fig. 2 shows τ_1^c in comparison with the τ_1^a cumulant distribution at NNLL. The most notable feature is the threshold $\theta(\tau_1^c - 1 + y)$ which shifts the τ_1^c result. This feature is associated with positivity of the jet mass $M_{\text{jet}}^2 = (\tau_1^c - 1 + y)s_J$ at LO. In addition to the threshold the τ_1^c curve increases more gently than the τ_1^a curve. This happens because the normalization factor for the beam axis q_B in τ_1^c differs from that in τ_1^a by a factor of $1/x$.

4. Summary

Factorization theorems for two jets in DIS were derived for three versions of 1-jettiness $\tau_1^{a,b,c}$ and numerical results were obtained up to NNLL order. The three 1-jettiness' measure particles relative to 3 different axes: jet axis, z-axis in the Breit frame and z-axis in CM frame. This leads to different dependence on transverse momentum. The factorization theorem is composed of hard, beam, jet, and soft functions currently known at an order that allows us to achieve NNLL accuracy. This means that in $\ln\sigma_c$ we resum terms: $\alpha_s L^2 (\alpha_s L)^k$, $\alpha_s L (\alpha_s L)^k$, and $\alpha_s (\alpha_s L)^k$ where $L = \log\tau_1$ and $k \geq 0$. Nonperturbative effects in the distribution appear as a power correction determined by a nonperturbative parameter Ω_1 when $\tau_1 Q \gg \Lambda_{QCD}$, which is universal for each of $\tau_1^{a,b,c}$. Our results contain the dominant singular terms appearing for small τ_1. To be accurate for larger $\tau_1 \sim 1$ we need to include non-singular terms which can be done by matching the fixed order cross section from the factorization theorem and full QCD. We leave this matching to future work.

Acknowledgments

The work of DK and IS is supported by the Office of Nuclear Physics of the U.S. Department of Energy under Contract DE-FG02-94ER40818, and the work of CL by DOE Contract DE-AC52-06NA25396 and by the LDRD office at Los Alamos.

References

[1] E. Farhi, Phys. Rev. Lett. **39**, 1587 (1977).

[2] A. Gehrmann-De Ridder, T. Gehrmann, E. W. N. Glover and G. Heinrich, Phys. Rev. Lett. **99**, 132002 (2007) [arXiv:0707.1285 [hep-ph]].

PoS(DIS 2013)158

[3] A. Gehrmann-De Ridder, T. Gehrmann, E. W. N. Glover and G. Heinrich, JHEP **0712**, 094 (2007) [arXiv:0711.4711 [hep-ph]].

[4] S. Weinzierl, Phys. Rev. Lett. **101**, 162001 (2008) [arXiv:0807.3241 [hep-ph]].

[5] S. Weinzierl, JHEP **0906**, 041 (2009) [arXiv:0904.1077 [hep-ph]].

[6] T. Becher and M. D. Schwartz, JHEP **0807**, 034 (2008) [arXiv:0803.0342 [hep-ph]].

[7] Y. -T. Chien and M. D. Schwartz, JHEP **1008**, 058 (2010) [arXiv:1005.1644 [hep-ph]].

[8] R. Abbate, M. Fickinger, A. H. Hoang, V. Mateu and I. W. Stewart, Phys. Rev. D **83**, 074021 (2011) [arXiv:1006.3080 [hep-ph]].

[9] R. Abbate, M. Fickinger, A. H. Hoang, V. Mateu and I. W. Stewart, Phys. Rev. D **86**, 094002 (2012) [arXiv:1204.5746 [hep-ph]].

[10] C. Adloff *et al.* [H1 Collaboration], Phys. Lett. B **406**, 256 (1997) [hep-ex/9706002].

[11] C. Adloff *et al.* [H1 Collaboration], Eur. Phys. J. C **14**, 255 (2000) [Erratum-ibid. C **18**, 417 (2000)] [hep-ex/9912052].

[12] A. Aktas *et al.* [H1 Collaboration], Eur. Phys. J. C **46**, 343 (2006) [hep-ex/0512014].

[13] J. Breitweg *et al.* [ZEUS Collaboration], Phys. Lett. B **421**, 368 (1998) [hep-ex/9710027].

[14] S. Chekanov *et al.* [ZEUS Collaboration], Eur. Phys. J. C **27**, 531 (2003) [hep-ex/0211040].

[15] S. Chekanov *et al.* [ZEUS Collaboration], Nucl. Phys. B **767**, 1 (2007) [hep-ex/0604032].

[16] V. Antonelli, M. Dasgupta and G. P. Salam, JHEP **0002**, 001 (2000) [hep-ph/9912488].

[17] M. Dasgupta and G. P. Salam, JHEP **0208**, 032 (2002) [hep-ph/0208073].

[18] M. Dasgupta and G. P. Salam, Phys. Lett. B **512**, 323 (2001) [hep-ph/0104277].

[19] D. Kang, C. Lee and I. W. Stewart, arXiv:1303.6952 [hep-ph].

[20] I. W. Stewart, F. J. Tackmann and W. J. Waalewijn, Phys. Rev. Lett. **105**, 092002 (2010) [arXiv:1004.2489 [hep-ph]].

[21] J. Thaler and K. Van Tilburg, JHEP **1202**, 093 (2012) [arXiv:1108.2701 [hep-ph]].

[22] Z. -B. Kang, S. Mantry and J. -W. Qiu, Phys. Rev. D **86**, 114011 (2012) [arXiv:1204.5469 [hep-ph]].

[23] Z. -B. Kang, X. Liu, S. Mantry and J. -W. Qiu, arXiv:1303.3063 [hep-ph].

[24] I. W. Stewart, F. J. Tackmann and W. J. Waalewijn, Phys. Rev. D **81**, 094035 (2010) [arXiv:0910.0467 [hep-ph]].

[25] S. Mantry and F. Petriello, Phys. Rev. D **81**, 093007 (2010) [arXiv:0911.4135 [hep-ph]].

[26] A. Jain, M. Procura and W. J. Waalewijn, JHEP **1204**, 132 (2012) [arXiv:1110.0839 [hep-ph]].

[27] G. P. Salam and D. Wicke, JHEP **0105**, 061 (2001) [hep-ph/0102343].

[28] C. Lee and G. F. Sterman, eConf C **0601121**, A001 (2006) [hep-ph/0603066].

[29] C. Lee and G. F. Sterman, Phys. Rev. D **75**, 014022 (2007) [hep-ph/0611061].

[30] V. Mateu, I. W. Stewart and J. Thaler, Phys. Rev. D **87**, 014025 (2013) [arXiv:1209.3781 [hep-ph]].

[31] Y. L. Dokshitzer and B. R. Webber, Phys. Lett. B **352**, 451 (1995) [hep-ph/9504219].

[32] R. Akhoury and V. I. Zakharov, Phys. Lett. B **357**, 646 (1995) [hep-ph/9504248].

[33] G. P. Korchemsky and G. F. Sterman, Nucl. Phys. B **437**, 415 (1995) [hep-ph/9411211].

PoS(DIS 2013)158